Contribution of magnetotail reconnection to the cross-polar cap electric potential drop

E. I. Gordeev,[1] V. A. Sergeev,[1] T. I. Pulkkinen,[2] and M. Palmroth[3]

Received 2 March 2011; revised 3 May 2011; accepted 13 May 2011; published 16 August 2011.

[1] Since the work of Dungey (1961), the global circulation pattern with two (dayside and nightside) reconnection regions has become a classic concept. However, the contributions of dayside and nightside sources to the cross-polar cap potential (PCP) are not fully understood, particularly, the relative role and specifics of the nightside source are poorly investigated both in quantitative and qualitative terms. To fill this gap, we address the contributions of dayside and nightside sources to the PCP by conducting global MHD simulations with both idealized solar wind input and an observed event input. The dayside source was parameterized by solar wind–based "dayside merging potential" $\Phi_d = L_{eff} V B_t \sin^4(\theta/2)$, whereas to characterize the nightside source we integrated across the tail the dawn-dusk electric field in the plasma sheet (to obtain the "cross-tail potential" Φ_n). For the idealized run we performed simulations using four MHD codes available at the Community Coordinated Modeling Center to show that contribution of the nightside source is a code-independent feature (although there are many differences in the outputs provided by different codes). Particularly, we show that adding a nightside source to the linear fit function for the ionospheric potential (i.e., using the fit function $\Phi_{fit} = K_d\Phi_d + K_n\Phi_n + \Phi_0$) considerably improves the fitting results both in the idealized events as well as in the simulation of an observed event. According to these simulations the nightside source contribution to the PCP has a fast response time (<5 min) and a modest efficiency (potential transmission factor from tail to the ionosphere is small, $K_n < 0.2$), which is closely linked to the primarily inductive character of strong electric field generated in the plasma sheet. The latter time intervals are marked by strongly enhanced nightside (lobe) reconnection and can be associated with substorm expansion phases. This association is further strengthened by the simulated patterns of precipitation, the R1-type field-aligned substorm current wedge currents and Hall electrojet currents, which are consistent with the known substorm signatures.

Citation: Gordeev, E. I., V. A. Sergeev, T. I. Pulkkinen, and M. Palmroth (2011), Contribution of magnetotail reconnection to the cross-polar cap electric potential drop, *J. Geophys. Res.*, *116*, A08219, doi:10.1029/2011JA016609.

1. Introduction

[2] The well-known global convection pattern of magnetospheric plasma fluxtubes, powered by the dayside and nightside reconnection processes, was proposed by *Dungey* [1961]. For southward interplanetary magnetic field (IMF), the Dungey cycle begins with reconnection of closed magnetospheric magnetic field lines with the IMF field lines in the subsolar region. The newly opened flux tubes are carried away in the antisunward direction by the solar wind flow and load the magnetotail lobes. Closed flux tubes in the tail, appeared due to merging of the lobe magnetic field lines, moves sunward in the plasma sheet and eventually returns to the dayside magnetopause [*Dungey*, 1961, 1963]. This description of magnetic flux transport cycle provides an explanation for the twin vortex ionospheric plasma flow and electric potential patterns. It has served as a basic paradigm for global magnetospheric circulation and continues to stimulate investigation of its origin and sources. Among all magnetospheric characteristics, the dawn-dusk electric potential drop (in other words, the polar cap potential, or PCP) plays a special role as it provides a global measure of the magnetospheric convection available in the ionosphere.

[3] Taken in steady state, the Dungey picture implies a mapping of potential along the nearly equipotential open field lines from the solar wind down to the ionosphere. This implies a strong solar wind control of the PCP, which was confirmed in statistical studies of the PCP variations [e.g., *Reiff et al.*, 1981; *Boyle et al.*, 1997; *Bristow et al.*, 2004] as well as in numerous investigations of different magnetic activity measures (see *Newell et al.* [2007] and *Lockwood et al.* [2009] for recent summaries of previous work and

[1]Department of Earth Physics, Saint Petersburg State University, St. Petersburg, Russia.
[2]School of Electrical Engineering, Aalto University, Espoo, Finland.
[3]Finnish Meteorological Institute, Helsinki, Finland.

0148-0227/11/2011JA016609

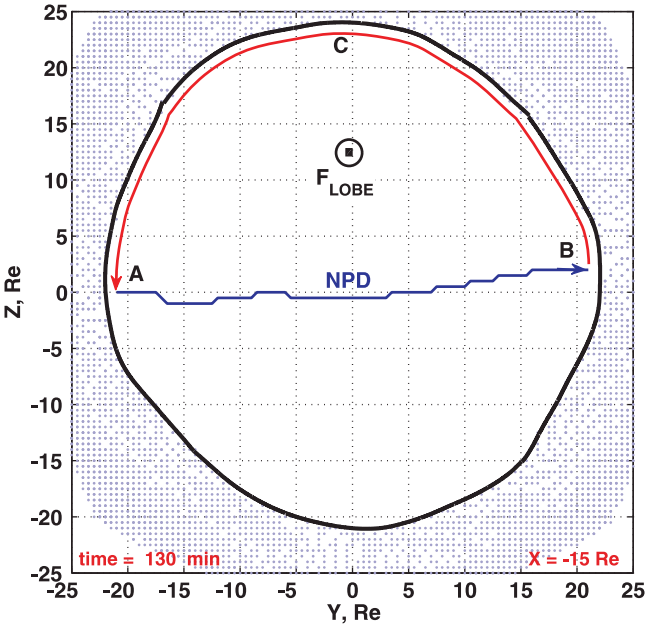

Figure 1. Magnetotail cross section at $X_{GSM} = -15$ Re with magnetopause (black line) defined as fluopause. The dots show cross sections of the flow lines traced from the solar wind. Curves with arrows visualize the contour AB used to calculate the cross-tail potential NPD and the contour ABCA used to calculate the tail magnetic flux and electric field circulation using Faraday's law.

extensive reference lists). However, such statistical studies, even if selecting slowly varying solar wind samples, always display a considerable scatter [see, e.g., *Bristow et al.*, 2004, Figure 6]. This suggests that solar wind electric field is not the only source of ionospheric potential, and nightside tail processes are certainly among the source candidates.

[4] *Siscoe and Huang* [1985] were the first to formally describe dayside and nightside reconnection processes as two independent sources. They developed the concept of moving adiaroic (no-flow across) polar cap boundaries with two short active segments, merging gaps (ionospheric projections of the dayside and nightside reconnection X lines). The concept was further developed by *Cowley and Lockwood* [1992]. However, until now there have been very few papers in which contribution of the nightside processes would have been evaluated in a quantitative way. Among them there are a few publications in which the contribution of the nightside reconnection has been approximately inferred from comparing observations of the polar cap flux changes and dayside reconnection rate [*Milan*, 2004; *Milan et al.*, 2007] or using SuperDARN convection estimates at the polar cap boundary [*Hubert et al.*, 2006]. In this (indirect) way the contribution of the tail reconnection processes to the cross-polar cap potential drop has been inferred to be significant, sometimes contributing up to 100 kV [*Milan et al.*, 2007]. A good coverage of the substorm bulge by SuperDARN observations of convection is extremely rare during strong substorms, but direct observations of moderate convection enhancements (up to 40 kV [*Grocott et al.*, 2002]) were shown for a weak substorm event. Finally, a statistical study by *Lockwood et al.* [2009] demonstrated that the use of a second independent variable (in this case the tail open magnetic flux) in addition to the solar wind electric field improves significantly the prediction of the observed polar cap potential variations. A direct quantitative evaluation of the efficiency of the nightside reconnection in contributing to the polar cap potential still awaits to be done.

[5] Since the cross-tail electric field is closely linked to the magnetic flux transport in the tail, it seems most natural to use it as a physical parameter to quantitatively characterize the nightside source. Unfortunately, this quantity cannot be directly inferred from observations. The best way of estimating this integral measure, the cross-tail potential $\Phi_n = \int E_y d_y$ in the plasma sheet, can currently be realized only from global MHD simulations. The goal of the present work is to demonstrate the influence of the nightside source on the cross-polar cap potential and to study its characteristics under varying conditions using global MHD model results.

2. Methodology

[6] We use the global MHD simulation results provided by different codes (BATS-R-US, Open GGCM, GUMICS and LFM) available at the Community Coordinated Modeling Center (CCMC), operating at NASA GSFC [http://ccmc.gsfc.nasa.gov]. All codes solve numerically the ideal MHD equations, whereas each of them has specific features in the numerical methods used in solvers; for the code descriptions see *Powell et al.* [1999] (BATS-R-US), *Raeder* [2003] (Open GGCM), *Janhunen* [1996] (GUMICS) and *Lyon et al.* [2004] (LFM).

[7] In this study we use both artificial solar wind input and observed event simulations. Using artificial input with step-like changes of the external driver facilitates identification of the different phases of magnetospheric dynamics, e.g. tail loading and unloading phases, as well as separation of the polar cap potential response in relation to dayside and nightside drivers. The four codes have been run with identical input and comparable resolution to isolate code-independent features in their output. As a quantitative tool to separate contributions of different sources we use multiple regression analysis, which also allow us to compare the driver responses in the artificial and observed events.

[8] Following *Milan* [2004] and *Lockwood et al.* [2009], we use $\varepsilon = VB_t \sin^4(\Theta/2)$, where V is the solar wind velocity, B_t transverse component of IMF, and Θ the IMF clock angle, to formally parameterize the dayside merging electric field. To convert it to a potential, we multiply the electric field by the effective reconnection line length $L_{eff} = 7$ Re [*Milan*, 2004] to get $\Phi_d = \varepsilon L_{eff}$.

[9] To characterize the nightside driver, we compute the integrated Earthward flux transfer in the plasma sheet. Specifically, we integrate the y component of electric field from dawn to dusk, i.e., the nightside potential drop (NPD) $\Phi_n = -\int (\mathbf{V} \times \mathbf{B}) \cdot \mathbf{dy}$ between the dawn and dusk magnetopause (points A and B in Figure 1). To find the magnetopause, we follow the approach of *Palmroth et al.* [2003] and construct at each time step the fluopause, a surface defined by innermost flow lines starting from solar wind and draping the magnetotail. A magnetopause contour (ACB in Figure 1) defined in such a way has also been used to compute the tail magnetic flux F at the same distance (see

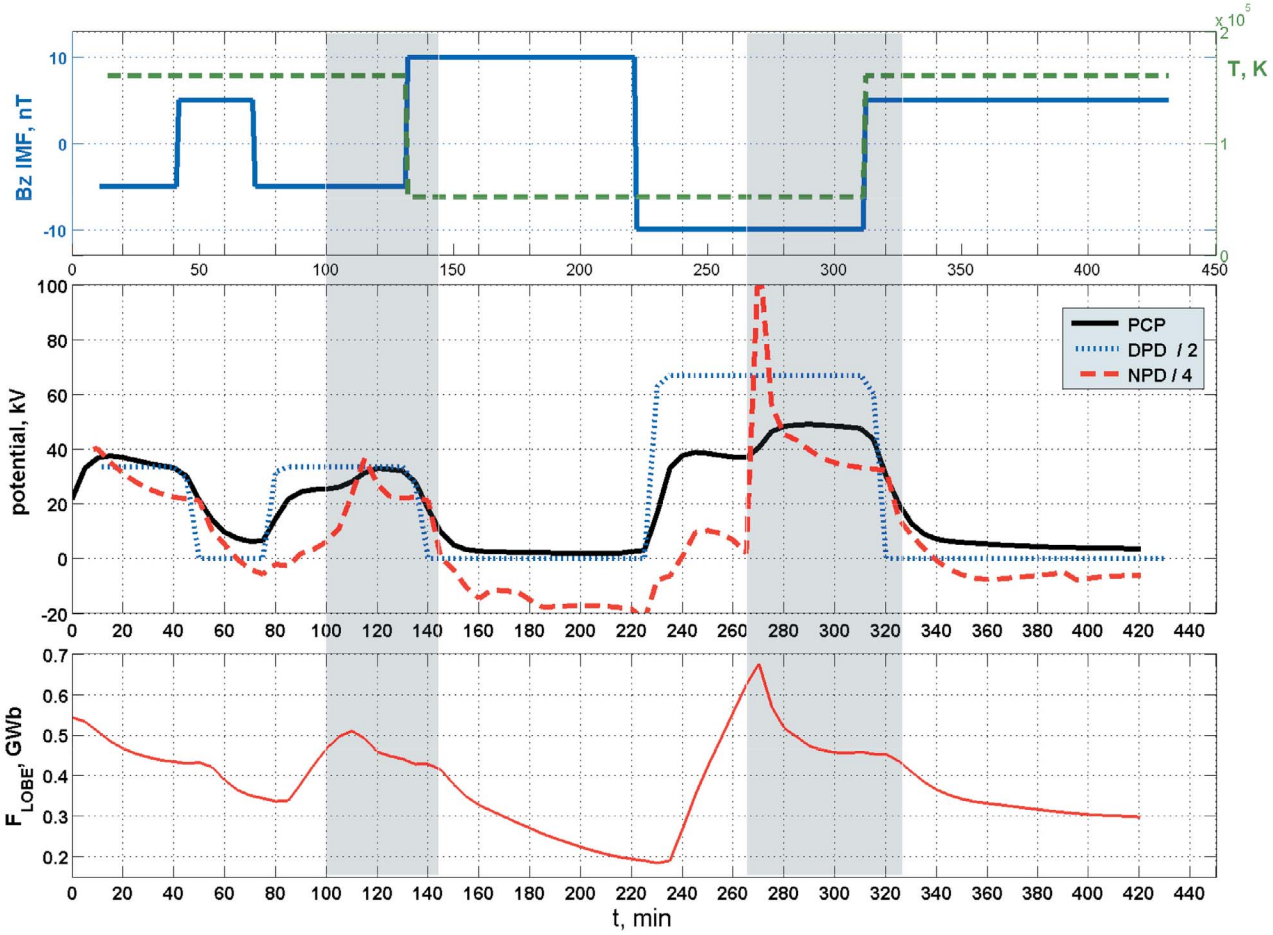

Figure 2. Simulation results for BATS-R-US code with uniform ionosphere. (top) B_z IMF (solid) and SW proton temperature (dashed) time-shifted to X_{GSM} = 10 Re with solar wind velocity. (middle) Variations of cross-polar cap potential in the ionosphere (solid), solar wind "dayside potential drop" (DPD) divided by 2 (blue dotted line) and cross-tail potential (NPD) divided by 3 (red dashed line). (bottom) Variations of tail lobe magnetic flux. Shaded area marks the time periods of substorm expansion phase (unloading periods under southward B_z).

also *Shukhtina et al.* [2009] for details of flux calculations), an important parameter to address the origin of the enhanced nightside electric field.

[10] The near-Earth neutral line has a complicated shape and it is extremely dynamic, thus the cross-tail potential may vary with distance. However, evaluation of the cross-tail potential at fixed distances from $X = -10$ to -25 Re box showed relatively weak changes, with variations less than 20%. Therefore, in the following this quantity was determined at a fixed cross-section distance at $X = -15$ Re.

[11] Every MHD simulation provides also an electric potential distribution in the ionosphere, from which we compute the cross-polar cap potential in the ionosphere (PCP, or Φ_{ion}). It was defined as the difference between the maximum potential values at dawn and minimum potential values at dusk, found in the centers of corresponding convection cells. To analyze quantitatively and compare contributions of nightside and dayside sources, we seek for a fit function for ionospheric potential drop in the form:

$$\Phi_{fit} = K_d \Phi_d + K_n \Phi_n + \Phi_0 \quad (1)$$

where K_d and K_n are linear regression coefficients, and Φ_0 represents a free term, usually interpreted as a viscous-like potential contribution. Note that K_d and K_n have a sense of transmission factors, determining which fraction of the corresponding potential is participating in generating the full ionospheric potential.

3. Simulation Results

[12] We used four different global MHD models, all run at comparable grid resolution, with identical solar wind and interplanetary magnetic field input parameters, all providing output at the same 5 min time resolution. Some solar wind input parameters were fixed, including solar wind plasma density N = 20 cm^{-3}, solar wind velocity $V_x = -300$ km/s, $V_y = V_z = 0$, interplanetary field $B_x = B_y = 0$, and the terrestrial dipole tilt angle $\Theta = 0$. The IMF B_z component variation consists of six time intervals with constant B_z and step-like changes in between. It includes (see Figure 2, top): $B_{z1} = -5$ nT between 00:00 and 00:30 hours, $B_{z2} = 5$ nT between 00:31 and 01:00, $B_{z3} = -5$ nT between 01:01 and

Table 1. Results of Multiple Linear Regression Analysis and Estimated Time Delays

Run Number, MHD Code	Ionospheric Model	CC (rmse) $\Phi_{SW} \rightarrow \Phi_{PC}$	CC (rmse) $\Phi_{fit} \rightarrow \Phi_{PC}$	CC (rmse) $\Phi_{Lock} \rightarrow \Phi_{PC}$	K_n	K_d	Φ_0	Δt(min) $\Phi_{SW} \rightarrow \Phi_{PC}$
1, BATS-R-US (real event)[a]	auroral	0.67 (12.1)	0.87 (7.8)	0.77 (10.5)	0.12	0.33	21	10
2, BATS-R-US[b]	auroral	0.88 (12.3)	0.98 (5.7)	0.95 (8.2)	0.16	0.32	6.1	10
3, BATS-R-US[c]	uniform	0.91 (6.9)	0.98 (3.1)	0.95 (5.0)	0.09	0.23	3.7	10
4, Open GGCM[d]	uniform	0.73 (32.3)	0.91 (19.8)	0.92 (19.1)	0.46	0.39	70	15
5, GUMICS[e]	uniform	0.87 (3.9)	0.88 (3.7)	0.95 (2.6)	0.02	0.11	13.5	5
6, LFM[f]	uniform	0.88 (22.0)	0.96 (13.0)	0.92 (18.5)	0.19	0.65	15.7	15

[a]Victor_Sergeev_060508_1 (BATSRUS).
[b]Evgeny_Gordeev_110309_1 (BATSRUS).
[c]Evgeny_Gordeev_110309_2 (BATSRUS).
[d]Evgeny_Gordeev_051810_1 (Open GGCM).
[e]Evgeny_Gordeev_051810_2 (GUMICS).
[f]Evgeny_Gordeev_051810_3 (LFM).

02:00, B_{z4} = 10 nT between 02:01 and 03:30, B_{z5} = −10 nT between 03:31 and 05:00 and, finally, B_{z6} = 5 nT between 05:01 and 07:00. In addition, the ion temperature changes have been chosen to satisfy the Rankine-Hugoniot conditions at tangential discontinuities (with $T = 1.6 \cdot 10^5$ K for $B_z = \pm 5$ nT and $T = 5.2 \cdot 10^4$ K for $B_z = \pm 10$ nT). In every simulation we used the same ionospheric model with uniform integral conductivity Σp = 7 Mho (Pedersen conductivity) and Σh = 7 Mho (Hall conductivity). We start from brief presentation of BATS-R-US model results shown in Figure 2 (for run 3 in Table 1), and then emphasize the similarities between four code simulations, as summarized in Figure 3 and Table 1.

3.1. Identification of PCP Response to the Nightside Driver

[13] In the case of idealized input, the MHD models demonstrate a nearly step-like response of the ionospheric potential PCP (Φ_{ion}) to the step-like changes of the IMF B_z (Figure 2, middle). The potential shows a nearly 10 min time delay after the estimated time of solar wind B_z arrival at X = 10 Re. After increasing in response to the IMF change, the PCP stays at this level while the tail lobe magnetic flux F continues to grow (loading phase). However, Figure 2 clearly shows an additional ionospheric potential increase starting simultaneously with the tail flux F decrease (the unloading phase).

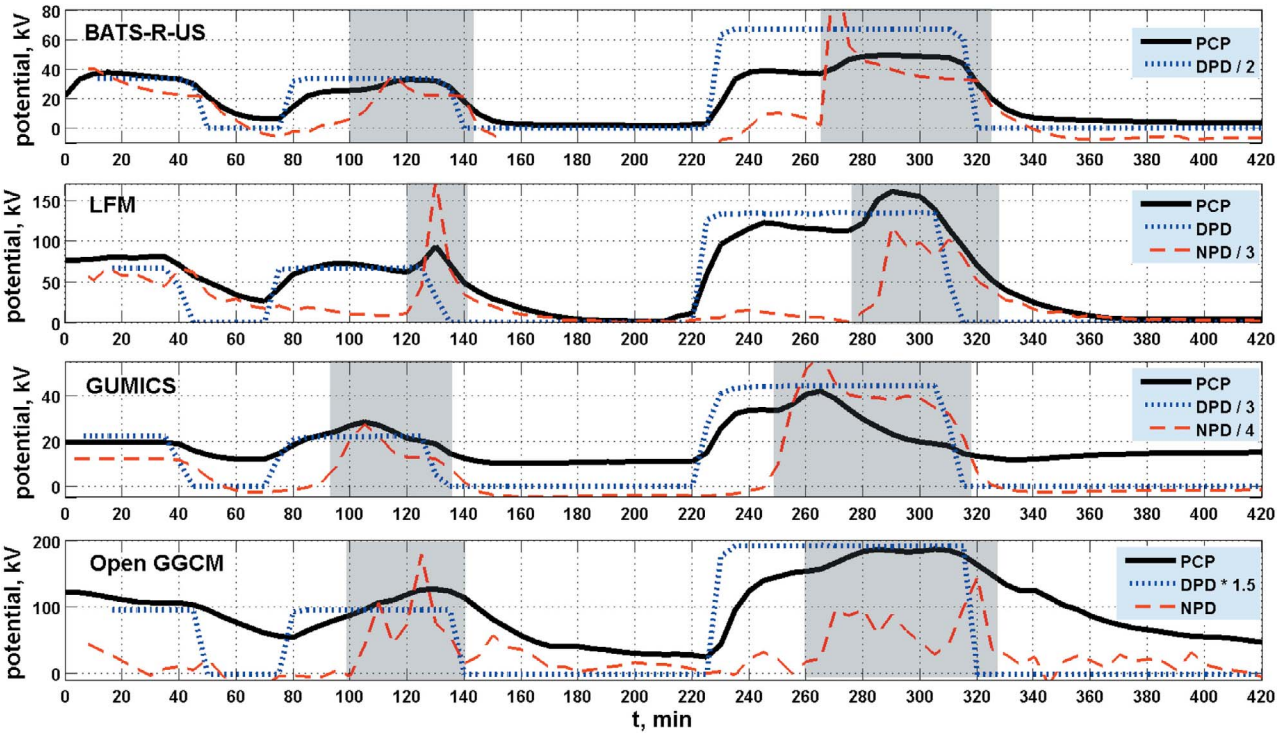

Figure 3. Results of different MHD codes which simulated the same artificial event. Each panel shows the ionospheric voltage (PCP, black solid line), solar wind "merging voltage" (DPD, blue dotted line), and "cross-tail voltage" (NPD, red dashed line). Shaded areas indicate the time periods of substorm expansion phase defined based on the unloading of tail magnetic flux.

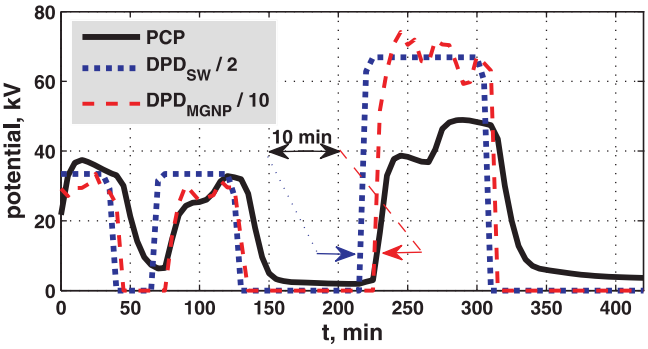

Figure 4. Time variations of electric potentials, including cross-polar cap potential in the ionosphere (PCP, black line); "dayside merging potential" transferred to $X = 10$ Re (DPD_{SW}, based on solar wind parameters, blue dotted line); and dayside merging potential (DPD_{MGNP}, red dashed line) estimated using direct integration of electric field in the equatorial plane on the subsolar portion ($X > 0$) of dayside magnetopause surface.

[14] In this run, two isolated episodes of strongly enhanced nightside reconnection (substorm expansions) can be identified starting at $t = 105$ min and $t = 270$ min. At these times, the activation of magnetic reconnection at 12–15 Re in the magnetotail results in fast plasma outflows, as well as plasmoid formation, growth and tailward ejection. These episodes are also seen as sharp decreases of the tail magnetic flux which continue until the end of the southward IMF B_z intervals, and which are further decreased after the northward IMF turning. Another impressive signature of nightside reconnection is the impulsive increase of the flux transport in the tail. In Figure 2 the flux transport is seen as impulsive increases of the cross-tail potential (NPD), starting from nearly zero values during the growth phase and reaching ~160 kV and ~400 kV peaks, correspondingly, at the two substorm expansion onsets. They also resulted in small but distinct changes of the cross-polar cap potential: the PCP increased from 25 kV to 33 kV during the first substorm and from 37 kV to 49 kV during the second substorm (both showing about ~25% increase). It is remarkable, that, in spite of the large differences of ionospheric potential magnitude in different codes (Figure 3 and Table 1), all models result in roughly the same relative PCP increase (about 20–30%) after switching on the near-Earth nightside reconnection.

[15] The last column in Table 1 shows a rough estimate of time delay between estimated appearance of IMF signal at $X = 10$ Re (dayside magnetopause distance) and the following PCP sharp increase. The obtained 10–15 min delay (Figure 4), is consistent with previous empirical estimates [e.g., *Sergeev et al.*, 1986; *Turner et al.*, 1998]. It is probably formed by the additional time required for the southward IMF front to propagate through the magnetosheath and to form and keep the magnetic barrier for initiation of the dayside merging. This is confirmed by comparison of solar wind–based "merging potential" with actual potential drop at the dayside magnetopause presented in Figure 4. It is interesting to note that for the drop of the dayside potential associated with the south-north IMF turning, the time delay between the solar wind is shorter, less than 5 min, which is the time resolution in our study.

[16] Table 1 summarizes the results of linear multiple regression analysis, results for 4 different codes with the same input and ionospheric models are placed in rows 3–6. (Two upper lines include the BATS-R-US results for two more runs briefly discussed later). The correlation coefficients (CC) and standard deviations (rmse) allow to compare how well the PCP is reproduced based on only dayside source fits (column 3, also including the free term Φ_0) compared to using both dayside and nightside sources (column 4, using the fit function given in equation (1)). In virtually all cases use of fitting function including the cross-tail potential in equation (1) shows a significant improvement in the polar cap potential prediction. For example, in the case of the BATS-R-US run (Figure 2), the correlation coefficient (CC) increases from 0.87 to 0.98 whereas the standard deviation error (rmse) drops from 12.3 to 5.4 kV. The free term in equation (1) can be interpreted as the viscose-like contribution to PCP and its value is about 4 kV in this run.

3.2. MHD Simulation With a Variable Ionospheric Conductivity: Details of Ionospheric Potential Response to the Nightside Driver

[17] We also run the BATS-R-US simulation with the same idealized input but different ionospheric model (auroral ionosphere model, row 2 in the Table 1) to include effects of variations of the ionospheric conductivity, which also depend on the magnetospheric electron precipitation [*Raeder*, 2003]. Comparison of two runs shows that with the auroral conductivity model, the cross-polar cap potential is about 30% larger than in the uniform conductivity case. Although precipitating electrons increase the ionospheric conductivity locally in the auroral oval (Figure 5), the conductivity averaged over the entire ionosphere is smaller than the 7 Mho used in the fixed conductivity model. The smaller conductivity may qualitatively explain the transpolar voltage increase in case if the potential source works like a current generator applied to conductive ionosphere. It is worth noting that, whereas the ionospheric potentials differ between these two simulations, the values of the tail magnetic flux and cross-tail potential are similar, demonstrating the absence of strong electric coupling between ionosphere and midtail plasma sheet flux transfer.

[18] The simulation results for variable auroral conductivity are suitable for analysis of the details of the ionospheric response (precipitation, field-aligned currents and electric field changes) during times when the ionospheric potential changes due to the sharply enhanced cross-tail potential. Figure 5 demonstrates this response during the strongest burst of cross-tail potential in BATS-R-US simulation, which started at $t = 265$ min and reached the 400 kV peak at $t = 270$ min. As already mentioned earlier, the ionospheric response to these bursts of magnetotail flux transport is modest. Therefore, to illustrate the changes visually, we show in the center and right columns of Figure 5 differential patterns of the conductivity (to visualize precipitation), field-aligned and ionospheric currents, with their values at $t = 265$ min (just before the start of near-Earth reconnection in the tail) subtracted. The total values at $t = 265$ min are shown at the left column of Figure 5 to

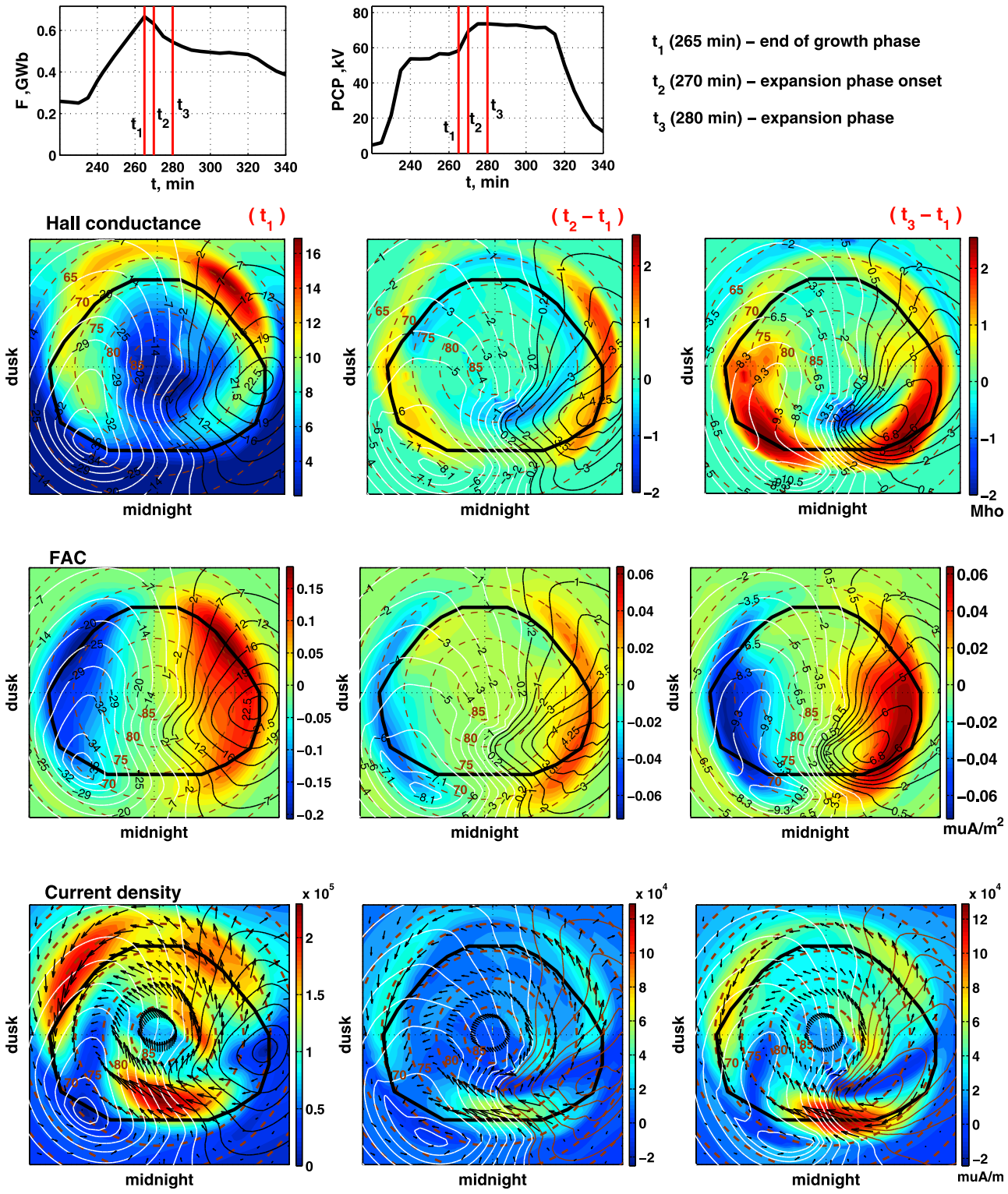

Figure 5. Ionospheric signatures of "MHD substorm expansion phase" during run 2. Panels in the top row characterize the "MHD substorm onset" and the times for which convection differential plots are shown. All other plots include the electric potential patterns in the ionosphere for these three times with superimposed color-coded distributions of Hall integral conductivity in the ionosphere (second row), field-aligned currents (third row), and ionospheric current density with superposed current vectors (fourth row). The thick line indicates the polar cap boundary at the initial time t_1. Note that left column shows the total potential and total conductance/current distribution at the end of growth phase, whereas middle and right columns show the differential plots with left column values subtracted.

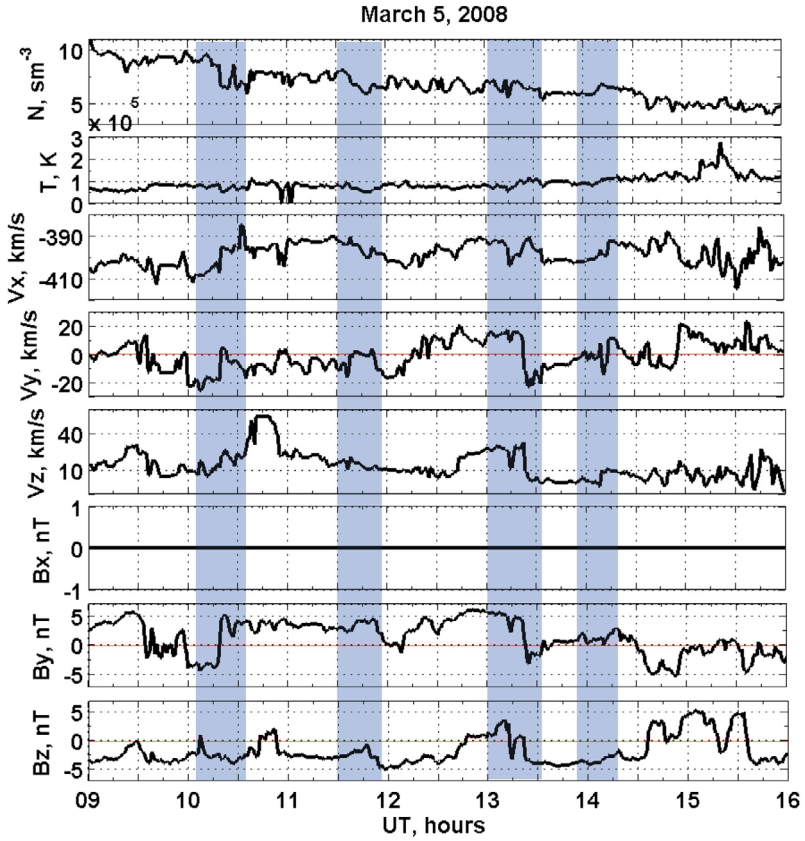

Figure 6. Solar wind input for 5 March 2008 event. Shaded areas indicate time periods of substorm expansion phase in the simulation results.

characterize the preonset distributions (note the scale changes between the total and differential patterns).

[19] The strongest changes in the ionosphere during the episode of enhanced magnetotail reconnection, as expected, are observed in the nightside portion of the auroral oval. The most interesting is the strongly enhanced convection in the "nightside merging gap", which is located between 21 and 03 hours MLT and have associated 15 kV potential drop. Note, that convection changes are observed globally, everywhere in the high latitude region. The entire global twin vortex pattern with convection concentrated in the nightside convection throat resembles very much the nightside merging-related patterns predicted by *Cowley and Lockwood* [1992]. Associated with this convection pattern is the R1 sense system of field-aligned currents. Although the peak current densities are observed near the edges of the nightside gap (near the foci of the convection vortices) which resemble the well-known substorm current wedge currents [*McPherron et al.*, 1973], the field-aligned currents are actually spread in the azimuthal direction and are observed in a wide MLT sector near the auroral zone convection reversal. The total additional FAC current is about 0.25 MA. The ionospheric currents have a clear enhancement in the convection throat region, where we see predominantly westward current, resembling the ionospheric closure of the substorm current wedge. The total current in this westward electrojet is about 0.3 MA.

[20] Having found these apparent parallels with the substorm expansion signatures (westward electrojet and substorm current wedge, convection throat), it was discouraging to observe the Hall conductivity pattern whose enhancements were concentrated in the premidnight and especially postmidnight sectors, in the regions of enhanced and azimuthally spread field-aligned currents, rather than in the convection throat and substorm current wedge, where the strong precipitation in the auroral bulge is observed during the substorm. This discrepancy probably shows a shortcoming of the MHD simulations in which the kinetic effects important for particle acceleration and precipitation into the auroral bulge are not properly included. This, of course, influences also the field-aligned and ionospheric current distribution and magnitudes, and thus the simulated ionospheric substorm signatures are not fully consistent with the observed electrodynamic substorm signatures in the ionosphere.

3.3. Observed Event Simulation

[21] The nightside source contribution to the ionospheric potential is clearly and repeatedly seen in simulations with artificial solar wind input. To reveal this effect in an observed event simulation is a more difficult but challenging task. For this purpose we have used the simulation performed for March 5, 2008 between 09 and 16 h UT.

[22] During this time period (Figure 6) the mostly southward IMF B_z was observed (with a few northward excursions), resulting in continuously high magnetic activity, the AE index was changing at around 400 nT level. Four substorms with onsets at 10h05m, 11h30m, 13h00m, 13h55m

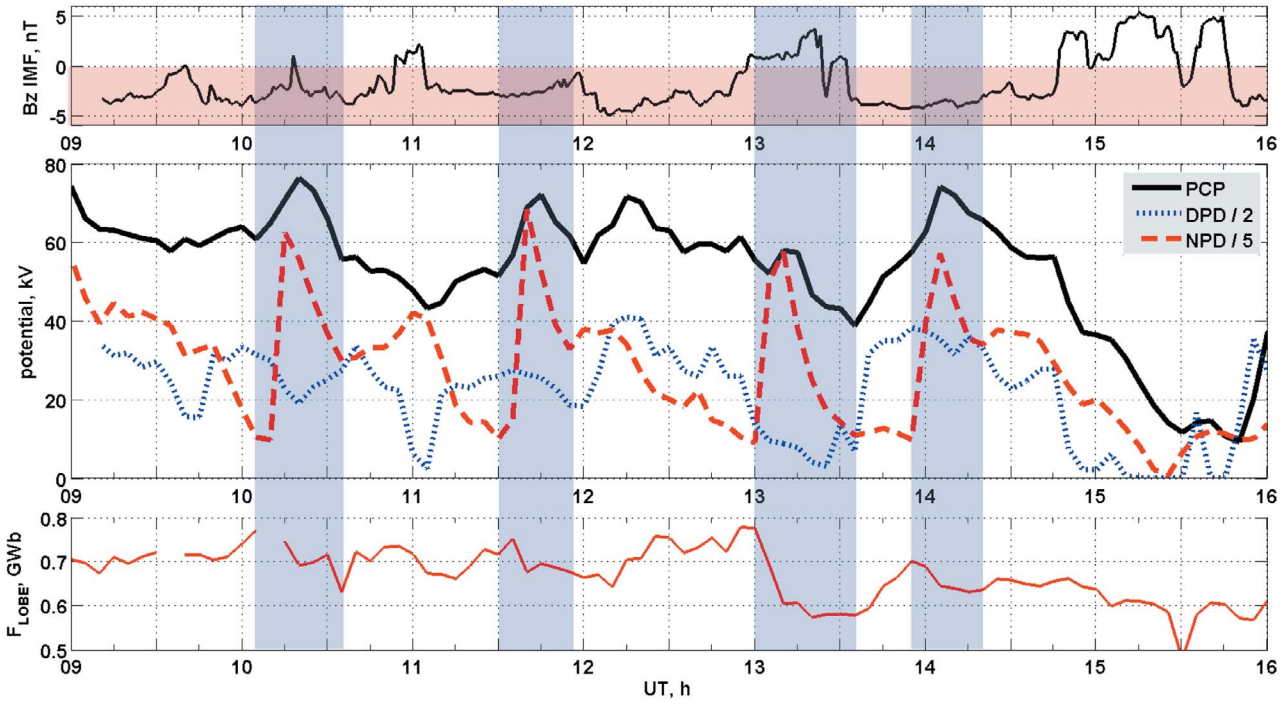

Figure 7. Observed event simulation results (run 1) in the same format as in Figure 4.

have been identified in this simulation. At these times one can see sharp intensifications of the cross-tail potential and corresponding increase of the ionospheric potential values (Figure 7).

[23] Regression analysis results for this event are presented in the first row of Table 1. Similarly to the artificial input runs, the potential shows a significant dependence on the dayside merging electric field (CC ~ 0.67). Similarly, addition of the nightside source to the fit function improves the correlation coefficient from 0.67 to 0.87 and reduces the standard deviation from 12.1 to 7.8 kV. The transmission coefficient in this case is also low (K_n = 0.12). A major difference is the generally smaller correlation and the 3.5 times larger free term in the fit function (viscous-like potential Φ_0 = 21 kV) as compared to the artificial run 2.

4. Discussion

[24] We analyzed a series of MHD simulation runs intended to separate the contributions of the dayside merging process and of the nightside tail reconnection to the convection pattern in the ionosphere and, specifically, to separate their contributions to the cross-polar cap electric potential (PCP). The artificial input runs allowed us to isolate easily the episodes of fast unloading in the tail and to identify the corresponding PCP increases at these times, which were of the order of 20–30% compared to the pre-onset PCP values.

[25] The observational data for the contribution of the nightside reconnection are very scarce, because the nightside convection pattern is rarely observed in isolation (without intense dayside merging process), and because of radio wave absorption and suppression of electric field in the regions of enhanced conductivity within the auroral bulge. In rare fortunate cases, like those reported by *Grocott et al.* [2002] (a small substorm under northward IMF), a twin vortex potential pattern with vortex centers at near-midnight polar cap boundary was observed, resembling the simulation results shown in Figure 5. The potential drop reported in that study was however significant, about 40 kV, considerably larger than in our simulation. At the same time, *Kullen et al.* [2010, Figure 7] used DMSP-based reconstruction of the electric potential and reported a very modest enhancement of about 10–15 kV during passes through the nightside polar cap region.

[26] Specific properties of the near-Earth tail reconnection are the large magnitude of the cross-tail "potential drop" and the relatively small transmission factor characterizing its input to the total polar cap potential (see K_n values in Table 1, ranging between 10 and 20%, except for OPEN code simulations). These properties are closely related to the primarily inductive character of the electric field in the substorm time plasma sheet. To prove this we calculated the circulation of convective electric field along the moving closed contour ABCA encircling the tail cross section (Figure 1). Specifically we calculated $\Phi_{ABCA} = -\int (\mathbf{V}^* \times \mathbf{B}) \cdot \mathbf{dl}$, where the $V^* = V - V_b$ is taken in the local contour frame, moving at velocity V_b. Consistent with Faraday's law, this quantity behaves nearly identically to the time derivative of the lobe magnetic flux F (see Figure 8 (bottom); the differences between these curves arises from an inaccurate estimation of V_b due to the large 5 min time steps). The outbursts of cross-tail potential are major contributors to the negative dF/dt variation during the unloading phase, which proves the primarily inductive character of these large electric fields during substorm times.

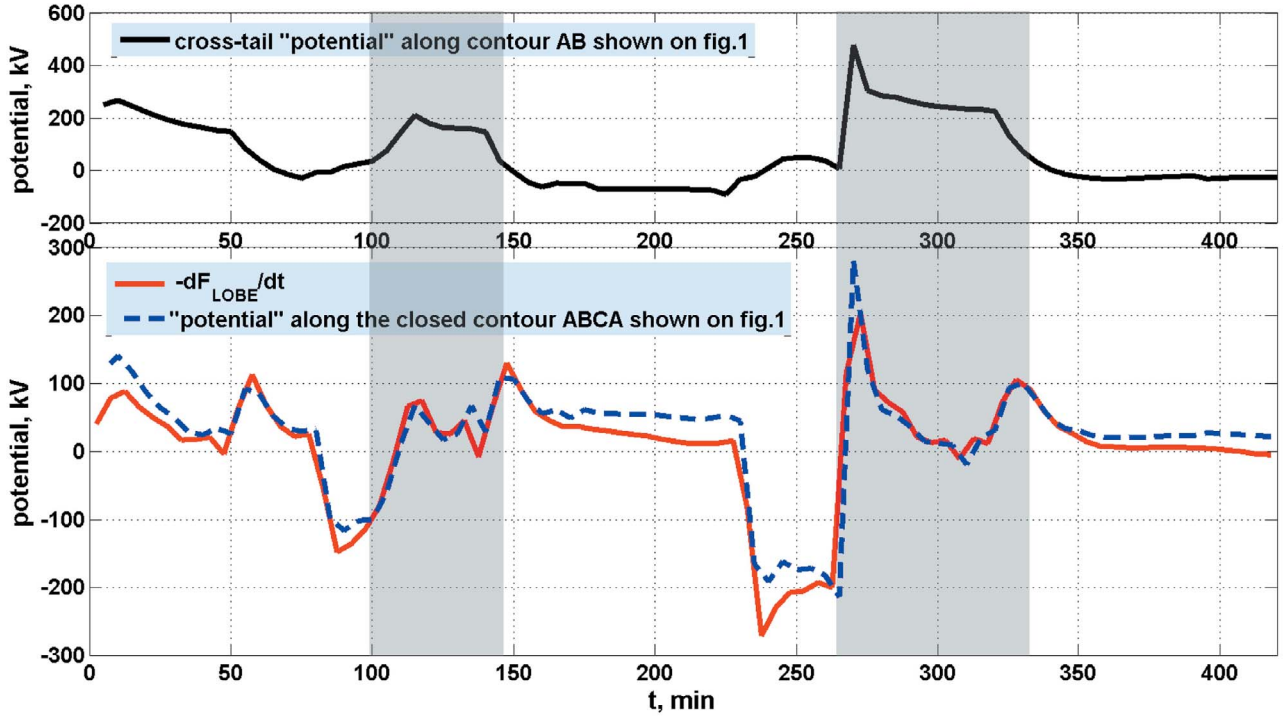

Figure 8. (top) Cross-tail potential and the comparison of electric field circulation (blue dashed line) with (bottom) time derivative of lobe magnetic flux (red line) in the tail cross section at $X = -15$ Re for run 3. Substorm expansion phase periods are shown by shaded bars.

[27] During such time periods with rapid changes of the ambient magnetic/plasma configuration, the character of electric coupling is very different from the case of stationary transport and electrostatic electric field mapping [*Semenov and Sergeev*, 1981]. Direct mapping of the electric potential along the magnetic field lines is no longer applicable and, as noted by *Heikkila and Pellinen* [1977], the appearance of the inductive electric field also changes the distribution of the potential electric fields, making the problem very difficult to solve. Instead of a direct potential mapping, several linked processes are directly involved. Particularly, the unsteady plasma motions change the magnetic configuration and plasma pressure distribution, which modifies the field-aligned currents and feed currents to the ionosphere, with the final equilibrium achieved only after a few Alfvén wave bounce times. The character of the magnetosphere-ionosphere coupling during such periods is therefore nonlocal and very difficult to solve, and MHD approach, although with the known limitations, provides a useful way to look at this problem.

[28] The fifth column in Table 1 presents regression results for an additional fit function in which, following suggestion by *Lockwood et al.* [2009], we used the square of the tail magnetic flux F^2 as the parameter characterizing the nightside driver. In that case $\Phi_{fit} = K_d\Phi_d + K_nF^2 + \Phi_0$. Whereas using this formulation brings some fit improvement, the result is typically worse compared to the fit using the nightside potential drop (column 4, except for GUMICS simulation). Therefore unlike the conclusions made by *Lockwood et al.* [2009], our simulation results show that it is not the tail magnetic flux F, but its time derivative dF/dt closely related to the cross-tail potential (Figure 8), which controls the contribution of processes in the nightside magnetotail to the cross-polar cap potential.

[29] To conclude, our investigation clearly reveals the contribution of the nightside reconnection process to the cross-polar cap ionospheric potential, which is a code independent feature observed in all global MHD simulation runs. This contribution is characterized by fast response and low efficiency (low K_n, ratio of the magnetotail contribution to the ionospheric potential) and related to the predominantly inductive character of strong reconnection-related electric fields in the nightside plasma sheet. The ionospheric manifestations during these "MHD substorms" include an additional twin vortex convection pattern with enhanced convection flow in the nightside merging gap and a substorm current wedge-like pattern of field-aligned currents combined with westward ionospheric currents in the high-latitude nightside auroral zone. Therefore, basic electrodynamics signatures of the tail reconnection are clearly seen in the ionosphere, and the tail processes obviously contribute to the cross-polar cap potential drop. Different MHD codes, however, demonstrate a large variability in the quantitative details, which will be investigated in future studies.

[30] **Acknowledgments.** E.G. and V.S acknowledge the Finnish Meteorological Institute for support during their stays in Helsinki. Their work was also supported by the EU grant (ECLAT 263325) as well as by the SPSU grant 11.38.47.2011. The research leading to these results has received funding from the European Research Council under the European Community's Seventh Framework Programme (FP7/2007-2013)/ERC Starting Grant agreement 200141-QuESpace. The work of M.P. is supported by the Academy of Finland.

[31] Masaki Fujimoto thanks the reviewers for their assistance in evaluating this paper.

References

Boyle, C., P. H. Reiff, and M. Hairston (1997), Empirical polar cap potentials, *J. Geophys. Res.*, *102*(A1), 111–126.

Bristow, W. A., R. A. Greenwald, S. G. Shepherd, and J. M. Hughes (2004), On the observed variability of the cross-polar cap potential, *J. Geophys. Res.*, *109*, A02203, doi:10.1029/2003JA010206.

Cowley, S. W. H., and M. Lockwood (1992), Excitation and decay of solarwind driven flows in the magnetosphere-ionosphere system, *Ann. Geophys.*, *10*, 103–115.

Dungey, J. W. (1961), Interplanetary magnetic fields and the auroral zones, *Phys. Rev. Lett.*, *6*, 47–48.

Dungey, J. W. (1963), The structure of the exosphere or adventures in velocity space, in *Geophysics, The Earth's Environment*, edited by C. De Witt, J. Hieblot, and L. Le Beau, Gordon and Breach, New York, p. 503.

Grocott, A., S. W. H. Cowley, J. B. Sigwarth, J. F. Watermann, and T. K. Yeoman (2002), Excitation of twin-vortex flow in the nightside high-latitude ionosphere during an isolated substorm, *Ann. Geophys.*, *20*, 1577–1601.

Heikkila, W., and R. Pellinen (1977), Localized induced electric field within the magnetotail, *J. Geophys. Res.*, *(10)*, 1610–1614.

Hubert, B., S. E. Milan, A. Grocott, C. Blockx, S. W. H. Cowley, and J.-C. Gerard (2006), Dayside and nightside reconnection rates inferred from IMAGE FUV and Super Dual Auroral Radar Network data, *J. Geophys. Res.*, *111*, A03217, doi:10.1029/2005JA011140.

Janhunen, P. (1996), GUMICS-3 A global ionosphere-magnetosphere coupling simulation with high ionospheric resolution, in *ESA Symposium Proceedings on 'Environmental Modelling for Space-Based Applications'*, *Eur. Space Agency Spec. Publ.*, *ESA SP-392*, 18–20.

Kullen, A., T. Karlsson, J. A. Cumnock, and T. Sundberg (2010), Occurrence and properties of substorms associated with pseudobreakups, *J. Geophys. Res.*, *115*, A12310, doi:10.1029/2010JA015866.

Lockwood, M., M. Hairston, I. Finch, and A. Rouillard (2009), Transpolar voltage and polar cap flux during the substorm cycle and steady convection events, *J. Geophys. Res.*, *114*, A01210, doi:10.1029/2008JA013697.

Lyon, J. G., J. A. Fedder, and C. M. Mobarry (2004), The Lyon–Fedder–Mobarry (LFM) global MHD magnetospheric simulation code, *J. Atmos. Sol. Terr. Phys.*, *66*, 1333–1350, doi:10.1016/j.jastp.2004.03.020.

McPherron, R., C. Russell, and M. Aubry (1973), 9. Phenomenological model for substorms, *J. Geophys. Res.*, *78*(16), 3131–3149.

Milan, S. E. (2004), Dayside and nightside contributions to the cross polar cap potential: Placing an upper limit on a viscous-like interaction, *Ann. Geophys.*, *22*, 3771–3777.

Milan, S. E., G. Provan, and B. Hubert (2007), Magnetic flux transport in the Dungey cycle: A survey of dayside and nightside reconnection rates, *J. Geophys. Res.*, *112*, A01209, doi:10.1029/2006JA011642.

Newell, P. T., T. Sotirelis, K. Liou, C.-I. Meng, and F. J. Rich (2007), A nearly universal solar wind-magnetosphere coupling function inferred from 10 magnetospheric state variables, *J. Geophys. Res.*, *112*, A01206, doi:10.1029/2006JA012015.

Palmroth, M., T. I. Pulkkinen, P. Janhunen, and C.-C. Wu (2003), Stormtime energy transfer in global MHD simulation, *J. Geophys. Res.*, *108*(A1), 1048, doi:10.1029/2002JA009446.

Powell, K. G., P. L. Roe, T. J. Linde, T. I. Gombosi, and D. L. de Zeeuw (1999), A solution–adaptive upwind scheme for ideal magnetohydrodynamics, *J. Comput. Phys.*, *154*, 284–309, doi:10.1006/jcph.1999.6299.

Raeder, J. (2003), Global magnetohydrodynamics—A tutorial, in *Space Plasma Simulation*, vol. 615, edited by J. Büchner, C. T. Dum, and M. Scholer, Springer, Berlin.

Reiff, P. H., R. R. Spiro, and T. Hill (1981), Dependence of polar cap potential on interplanetary parameters, *J. Geophys. Res.*, *86*(A9), 7639–7648.

Semenov, V. S., and V. A. Sergeev (1981), A simple semi-empirical model for the magnetospheric substorm, *Planet. Space Sci.*, *29*, 271–281.

Sergeev, V. A., N. P. Dmitrieva, and E. S. Barkova (1986), Triggering of substorm expansion by the IMF directional discontinuities: Time delay analysis, *Planet. Space Sci.*, *34*, 1109–1118.

Shukhtina, M. A., E. I. Gordeev, and V. A. Sergeev (2009), Time-varying magnetotail magnetic flux calculation: A test of the method, *Ann. Geophys.*, *27*, 1583–1591. [Correction, *Ann. Geophys.*, *28*, 415, doi:10.5194/angeo-28-415-2010, 2010.]

Siscoe, G. L., and T. S. Huang (1985), Polar cap inflation and deflation, *J. Geophys. Res.*, *90*(A1), 543–547.

Turner, N., D. Baker, T. Pulkkinen, H. Singer, F. Mozer, and R. Lepping (1998), High-altitude polar cap electric field responses to southward turnings of the interplanetary magnetic field, *J. Geophys. Res.*, *103*(A11), 26,533–26,545.

E. I. Gordeev and V. A. Sergeev, Department of Earth Physics, Saint Petersburg State University, St. Petersburg 198504, Russia. (evgeniy_gordeev@yahoo.com; v.sergeev victor@geo.phys.spbu.ru)

M. Palmroth, Finnish Meteorological Institute, PO Box 503, Helsinki FI-00101, Finland. (minna.palmroth@fmi.fi)

T. I. Pulkkinen, School of Electrical Engineering, Aalto University, PO Box 13000, Espoo FI-00101, Finland. (tuija.i.pulkkinen@aalto.fi)